The Radiometric Stability and Scaling of Collection 6 Terra- and Aqua-MODIS VIS, NIR, and SWIR Spectral Bands

David R. Doelling, Aisheng Wu, Xiaoxiong Xiong, Benjamin R. Scarino, Rajendra Bhatt, Conor O. Haney, Daniel Morstad, and Arun Gopalan

***Abstract*—The Moderate Resolution Imaging Spectroradiometer (MODIS) Calibration Team has recently released the Collection 6 (C6) radiances, which offer broad improvements over Collection 5 (C5). The recharacterization of the solar diffuser, lunar measurements, and scan mirror angle corrections removed most of the visible channel calibration drifts. The visible band calibration stability was validated over the Libyan Desert, Dome-C, and deep convective cloud (DCC) invariant Earth targets, for wavelengths less than 1 μm. The lifetime stability of Terra and Aqua C6 is both within 1%, whereas the Terra C5 degradation exceeded 2% for most visible bands. The MODIS lifetime radiance trends over the invariant targets are mostly within 1%; however, the band-specific target fluctuations are inconsistent, which suggests that the stability limits of the invariant targets have been reached. Based on Terra- and Aqua-MODIS nearly simultaneous nadir overpass (NSNO) radiance comparisons, the Terra and Aqua C6 calibration shows agreement within 1.2%, whereas the C5 calibration exceeds 2%. Because the MODIS instruments are alike, the same NSNOs are used to radiometrically scale the Terra radiances to Aqua. For most visible bands, the Terra-scaled and Aqua C6 radiances are consistent to within 0.5% over Dome-C, DCC, and for geostationary visible imagers having similar spectral response functions, which are used as transfer radiometers. For bands greater than 1 μm, only minor calibration adjustments were made, and the C6 calibration is stable within 1% based on Libya-4.**

***Index Terms*—Intercalibration, Moderate Resolution Imaging Spectroradiometer (MODIS), pseudoinvariant calibration sites (PICS), radiometric scaling.**

Manuscript received February 12, 2014; revised August 25, 2014; accepted January 21, 2015. This work was supported in part by the National Aeronautics and Space Administration Earth Science Enterprise Office through the Clouds and the Earth's Radiant Energy System and the Satellite Calibration Interconsistency Programs and in part by the National Atmospheric and Oceanic Administration Climate Data Records Program under Grant MOA IA1-1016.

D. R. Doelling is with the Climate Sciences Branch, NASA Langley Research Center, Hampton, VA 23681 USA (e-mail: david.r.doelling@nasa.gov).

A. Wu is with Sigma Space Corporation, Lanham, MD 20706 USA (e-mail: Aisheng.Wu@sigmaspace.com).

X. Xiong is with the Sciences and Exploration Directorate, NASA Goddard Space Flight Center, Greenbelt, MD 207713 USA (e-mail: xiaoxiong.xiong-1@nasa.gov).

B. R. Scarino, R. Bhatt, C. O. Haney, D. Morstad, and A. Gopalan are with Science Systems and Applications, Inc., Hampton, VA 23666 USA (e-mail: Benjamin.r.scarino@nasa.gov; rajendra.bhatt@nasa.gov; conor.o.haney@nasa.gov; Daniel.morstad@nasa.gov; arun.gopalan-1@nasa.gov).

Color versions of one or more of the figures in this paper are available online at http://ieeexplore.ieee.org.

Digital Object Identifier 10.1109/TGRS.2015.2400928

I. Introduction

THE Moderate Resolution Imaging Spectroradiometer (MODIS) imagers [1]–[3] onboard the Terra and Aqua satellites have been continuously scanning the Earth for over 13 and 11 years, respectively. The 36 spectral channels of the MODIS imager are used by the remote sensing and ocean- and land-use communities to retrieve cloud, aerosol, and surface properties. The MODIS Characterization Support Team (MCST) has just released the Collection 6 (C6) calibrated band radiances, which have mitigated all known calibration anomalies and are an improvement over the Collection 5 (C5) radiances. The onboard MODIS C6 visible channel calibration improvements were discussed by Wu *et al.* [4], as well as an assessment of the MODIS C5 visible channel radiometric temporal stability using the Libya-4 Desert, Dome-Concordia (Dome-C, located in Antarctica) pseudoinvariant calibration sites (PICS), and equatorial deep convective clouds (DCC). The first goal of this paper is to assess the MODIS C6 visible channel radiometric stability using the same Earth invariant target approach used to evaluate the C5 stability. The second goal of this paper is to provide Terra to Aqua-MODIS C6 visible channel radiometric scaling factors, which the reader can apply to retrieve consistent Terra- and Aqua-MODIS-based radiative, cloud, aerosol, and surface properties. Unless otherwise stated, reference to Terra or Aqua implies reference to their MODIS instruments.

This paper focuses on the MODIS visible (VIS) bands 1 (0.65 μm), 3 (0.47 μm), and 4 (0.55 μm); near-infrared (NIR) band 2 (0.86 μm); and shortwave infrared (SWIR) bands 5 (1.24 μm), 26 (1.38 μm), and 7 (2.12 μm). The SWIR band 6 (1.64 μm) is not considered, because most of the Aqua-MODIS band 6 detectors are nonfunctional. Other visible high-gain bands intended for ocean color and surface property retrievals are excluded from this study because they saturate over highly reflective Libya-4 and DCC targets. In this paper, the term "VIS" refers to wavelengths less than 1 μm, and the term "SWIR" refers to wavelengths greater than 1 μm. In this paper, the NIR is a subset of the VIS band.

A short summary of the MODIS C6 visible calibration is provided here. The MODIS onboard visible calibration monitoring relies on the solar diffuser (SD), the SD stability monitor (SDSM) [5], [6], lunar looks [7], and internal lamps located in the Spectroradiometric Calibration Assembly (SRCA) [8]. The

SRCA is not used because the lamp stability is not well known. The C5 radiometric stability monitoring and absolute calibration relied on the SD wavelength measurements normalized by those at the 0.94-μm wavelength of the SD to remove unwanted fluctuations due to its screen pinhole effects. The 0.94-μm wavelength of the SD, based on the SDSM measurements, was found not to degrade during the early part of the mission. Later, it was discovered that the 0.94-μm wavelength of the SD started to show noticeable degradations. In early 2009, it was found that the 0.94-μm SD degraded by 1.5% and 0.3% in Terra and Aqua, respectively; and the visible calibration coefficients were adjusted accordingly to offset the degradation. The greater degradation in Terra is due to the SD door being permanently in the open position beginning on July 2, 2003.

The prelaunch bidirectional reflectance distribution function (BRDF) of the scan mirror was initially used to characterize the angle of incidence (AOI) or the sensor response versus scan angle (RVS) in C5. The scan mirror degradation can be monitored at an AOI of 11.2° using lunar looks by employing a monthly spacecraft roll maneuver and at 50.2°, where the SD and SDSM ports are located. The Earth scan range is between 10.5° and 65.5°. For C5, a linear adjustment of the prelaunch RVS, based on the degradation difference between the SD and the lunar look, was used to define the degradation of the scan mirror. The C5 calibration coefficients were updated biweekly during forward processing of the MODIS radiances. For C6, the SD/SDSM and lunar measurements were reexamined over the entire MODIS record. A high-order polynomial regression was used to model the temporal degradation at both AOIs. The noise about the fit for the SD and lunar observations was within 0.3% and 0.5%, respectively. Deserts were used to define the temporal variation of the RVS dependence and are anchored to the lunar and SD degradations at their corresponding AOIs for a few shortest wavelength bands [9]. Thus, the C6 absolute calibration of bands 1–4 and 8–9 on Terra and bands 8 and 9 on Aqua is based on the early mission SD/SDSM and lunar measurements and tracked by the stability of Libya-4. The C6 absolute calibration of other bands is still based on the continuous SD/SDSM and RVS measurements [10], [11].

The fact that Terra and Aqua MODIS instruments are nearly identical and have the same band spectral response functions (SRFs) facilitates the possibility of radiometric scaling Terra visible radiances to the Aqua calibration reference. Doing so removes any residual calibration differences between the two instruments, which may have resulted from inaccuracies in the prelaunch BRDF characterization or the ground-to-on-orbit change in calibration.

Aqua-MODIS is chosen as the reference because the MCST claims that Aqua-MODIS is the better performing instrument [5]. The MODIS absolute calibration uncertainty in the early mission is within 1.7% and 1.8% for bands 1–4 for Aqua and Terra, respectively; whereas for bands 5–7 and 26, the uncertainty is within 1.8% and 2.6%, respectively [12]. In addition, based on both SD/SDSM and lunar measurements, the Terra visible sensors have degraded more rapidly over time than the Aqua sensors [4]. Currently, the Global Space-based Inter-Calibration System (GSICS) [13], which is an international organization dedicated to improve and uniformly calibrate operational satellite sensors, also uses Aqua-MODIS band 1 (0.65 μm) as their absolute calibration reference. Eventually, the Aqua-MODIS reference will be tied to the National Polar-Orbiting Operational Environmental Satellite System (NPOESS) Preparatory Program (NPP) Visible Infrared Imager Radiometer Suite (VIIRS) instrument. The VIIRS imager calibration will be then tied to more accurately calibrated future imagers. The absolute calibration, when it is known, can be then applied across radiometrically scaled imagers. Doing so will allow for consistent retrievals across imagers and for the production of multisatellite long-term climate data records.

This paper is organized as follows. Section II repeats the invariant Libya-4, Dome-C, and DCC target consistency analysis in order to evaluate the C6 stability. Section III radiometrically scales the Terra radiances to the Aqua-MODIS C6 reference calibration. The scaling factors are validated by comparing the Terra and Terra-scaled radiances with Aqua radiances using the same invariant Earth targets (see Section IV), and using geostationary (GEO) imagers as transfer radiometers (see Section V). Conclusions are presented in Section VI.

II. Comparison of MODIS C5 and C6 Stability

This section validates the MODIS SD/SDSM, lunar, and RVS C6 calibration improvements by evaluating the stability of the MODIS reflectances over the Libya-4, Dome-C, and DCC invariant Earth targets. The overall at-launch sensitivity of bands 3 (0.47 μm) and 4 (0.55 μm) was reduced by 30%, whereas that of bands 1 and 2 increased by 10%. For wavelengths greater than 1 μm, sensitivity degraded by 8% based on SD measurements. The C5 calibration coefficients corrected for the changes in sensitivity. However, the C5 Terra-MODIS calibration showed a wavelength-dependent degradation caused by the postlaunch drifts in the SD BRDF and RVS, which are corrected in C6 [10], [11]. The same Wu *et al.* [4] independent PICS evaluation of the MODIS calibration procedure was followed in this study. The same data points used in the C5 analysis are used for C6, except that the C6 record was extended. The Terra- and Aqua-MODIS C6 and C5 stability information, based on the PICS, is given in Table I. The C5 stability in Table I is from [4, Table 2]. The associated quadratic fit trend standard error is shown in Table II.

A. Libya-4 Desert

The Libya-4 (28.55° N, 23.39° E) top of atmosphere (TOA) near-nadir (view angles within 5°) 20 × 20 km spatial gridded instantaneous clear-sky reflectances are corrected using a BRDF model based on the first three years of measurements, which is the more stable part of the MODIS record [14], [15]. Measurement frequency is limited by the 16-day Terra or Aqua orbit repeat cycle. Clear sky is determined from a spatial uniformity threshold of the pixel-level reflectances. The Terra C6 calibration is an improvement over the C5 calibration because the lifetime trend for all bands is within 1% (see Table I). The exception is the 0.44-μm band, which degraded a few percent until 2009 and then recovered (see Fig. 1). The Aqua C6 radiances are stable for the first five years, and then, they slowly degrade for all bands. The Aqua

TABLE I
TERRA- AND AQUA-MODIS C5 AND C6 STABILITY IN PERCENT OVER THE RESPECTIVE SATELLITE LIFETIMES AS A FUNCTION OF BAND. THE DCC C6 DATA BEGIN AFTER JULY 2002 TO AVOID THE POOR DATA QUALITY BETWEEN 2000 AND 2001

MODIS Band		Terra						Aqua					
		Deserts		Dome C		DCC		Deserts		Dome C		DCC	
μm	#	C5	C6	C5	C6	C5	C6	C5	C6	C5	C6	C5	C6
0.44	**9**	-8.8	1.0					0.0	-1.3				
0.47	**3**	-6.3	0.0	-4.6	1.9	-3.5	0.2	0.7	-0.8	0.0	0.7	0.4	0.0
0.55	**4**	-1.2	0.1	-0.3	-0.2	-0.4	-0.3	0.5	-0.9	1.1	0.7	0.8	-0.1
0.65	**1**	-2.1	0.9	-1.6	0.8	-2.5	-0.1	0.0	-1.4	0.5	-0.0	-0.1	-0.9
0.86	**2**	-1.9	0.9	-2.9	2.0			0.0	-1.8	0.0	0.6		
1.24	**5**	0.4	0.5			2.6	1.6	-0.3	-0.7			1.3	0.8
1.38	**26**					1.4	0.8					0.6	0.9
2.12	**7**	-0.8	-0.3			0.5	1.7	0.1	-0.9			2.2	1.6

TABLE II
SAME AS TABLE I, BUT TREND STANDARD ERROR, IN PERCENT

MODIS Band		Terra						Aqua					
		Deserts		Dome C		DCC		Deserts		Dome C		DCC	
μm	#	C5	C6	C5	C6	C5	C6	C5	C6	C5	C6	C5	C6
0.44	**9**	1.2	1.3					1.4	1.4				
0.47	**3**	1.2	1.3	1.0	0.8	1.4	0.6	1.4	1.4	0.7	0.6	0.8	0.6
0.55	**4**	1.0	1.0	1.7	1.2	1.1	0.7	1.1	1.2	1.6	1.3	0.8	0.6
0.65	**1**	1.0	1.0	1.5	1.0	0.8	0.6	0.9	0.9	1.5	1.3	0.7	0.6
0.86	**2**	1.0	1.0	1.4	1.2			1.0	0.9	1.5	1.2		
1.24	**5**	0.9	1.3			1.3	0.6	0.9	0.9			1.6	0.9
1.38	**26**					1.8	1.0					2.1	1.3
2.12	**7**	2.1	2.1			2.8	1.8	1.9	1.8			5.0	3.4

C6 lifetime degradation ranges between -0.7% and -1.8%. The Aqua VIS and Terra and Aqua SWIR bands show a rapid increase and decrease in reflectance beginning in 2013, which is probably related to a short brightening event over Libya-4. Since the Terra VIS band calibration stability is based on Libya-4, therefore, it does not show this event. The Libya-4 trend standard error is within $\sim 1.4\%$ (see Table II). Considering both Terra and Aqua bands, only the Aqua 0.65- and 0.86-μm bands have lifetime C6 trends greater than the trend standard error.

B. Dome-C

Similarly, the high-altitude and exceedingly dry Dome-C (75.3° S, 123.4° E) TOA near-nadir (view angles within 5°) 20×20 km spatial gridded instantaneous clear-sky reflectances were normalized using a BRDF model based on the first three years of MODIS measurements [14], [16]. Although Dome-C has a greater surface reflectance than Libya-4, the large solar zenith angles (SZAs) reduce the signal-to-noise ratio over Dome-C. The Dome-C trend standard error is ~ 1.5 times the Libya-4 standard error in C5, except for the 0.47-μm band, and is comparable with Libya-4 in C6 after an improved BRDF correction is applied (see Table II). Similar to Libya-4, the Dome-C Terra and Aqua trends diverge after 2007 (see Fig. 2). However, the Aqua trends do not degrade, and Terra bands 2 and 3 show more of a positive trend. For this site, the Terra 0.47- and 0.86-μm bands have lifetime C6 trends greater than the trend uncertainty.

C. DCC

The DCC TOA pixel-level radiances over the tropics ($\pm 20°$ latitude) are identified by using a simple IR threshold and are normalized to overhead sun using *a priori* BRDF model [17], [18]. DCC identified pixels occupy $\sim 0.5\%$ of the tropics at any given time and are collectively analyzed monthly by tracking the probability distribution function mode of the overhead sun DCC pixel radiances. Typically, over 100 000 DCC pixels are identified monthly. Since DCC are nearly isotropic for near-nadir view, the corrections are much smaller than for either Libya-4 or Dome-C. DCC, above which extremely dry conditions prevail, are analyzed in near-overhead sun conditions

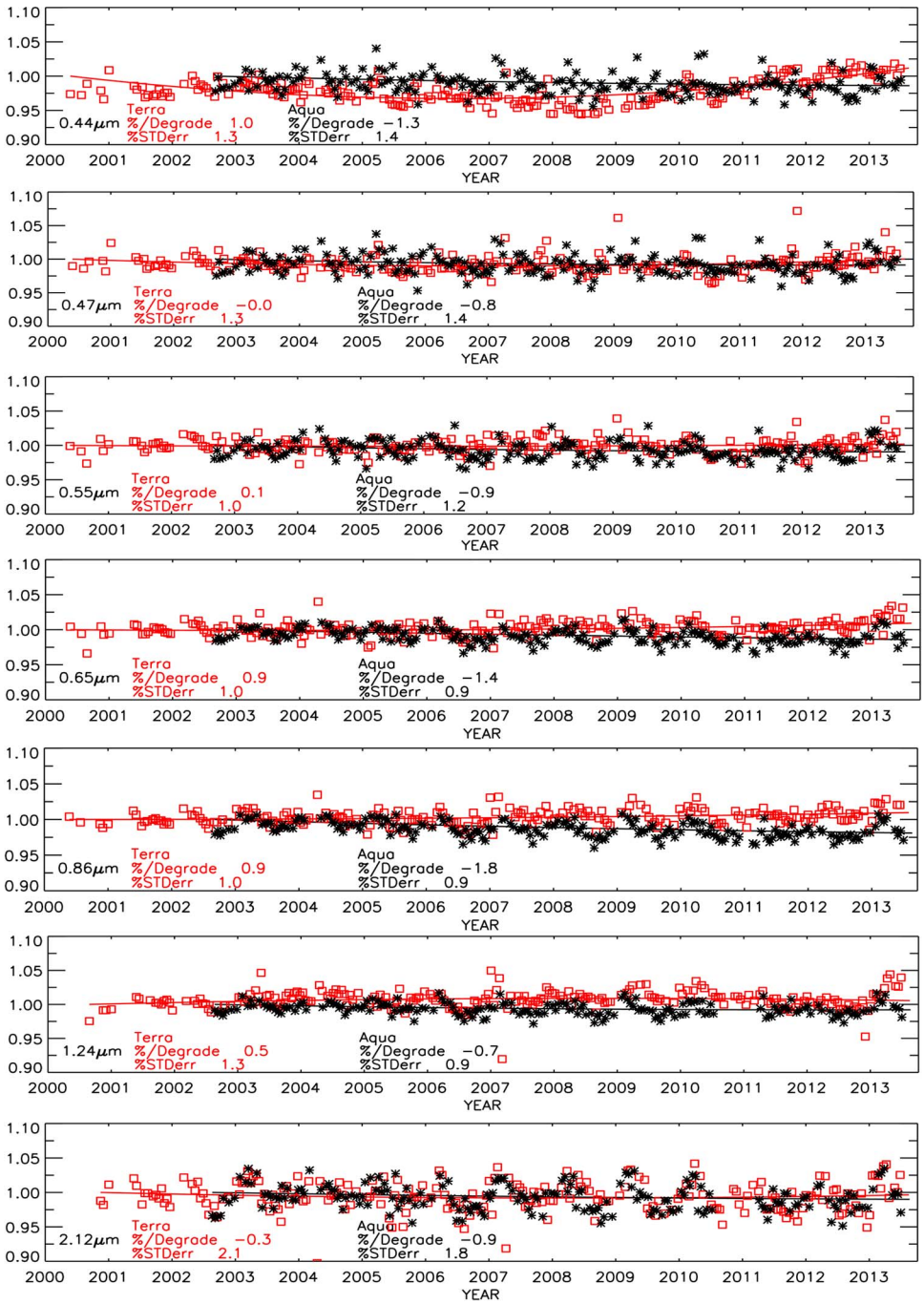

Fig. 1. Trends of Terra (red) and Aqua (black) normalized at-launch Libya-4 C6 reflectances for the bands listed in the lower left of each panel. Trends are computed using a second-order polynomial. Total lifetime degradation and trend standard error are given in percent.

and contain the brightest tropical scenes, thereby providing the greatest signal-to-noise ratio of the invariant Earth targets used in this study. The 0.86-μm channel pixel-level radiances saturate over bright DCC and cannot be calibrated using such a methodology. The dark Terra C6 band 0.47-, 0.55-, 1.24-, and 1.37-μm DCC radiances observed during 2000 are probably a result of poor data quality (see [4, Fig. 6]) and may not represent the true Terra trends. Therefore, only DCC data beginning in July 2002 are shown in Fig. 3. Most of the post-2008 Terra C5 VIS band degradations were removed in C6. In fact, the Terra C6 0.47-, 0.55-, and 0.65-μm trends are within 0.4%. For all bands, the C6 calibration is more stable than C5, except for the Terra 2.12-μm, Aqua 0.65-μm, and Aqua 1.38-μm bands. The Aqua C6 DCC band trends are more stable or similar to Terra, except for the 0.65-μm band. Remarkably, the DCC C6 trend standard error is less than the C5 standard error, thus confirming the improvement of the C6 calibration. The Terra 1.24-μm and Aqua 0.65-μm bands have degraded beyond the standard error for C6.

D. Summary

In general, the Terra and Aqua C6 VIS band trends diverge after 2007, with Aqua generally having more negative trends.

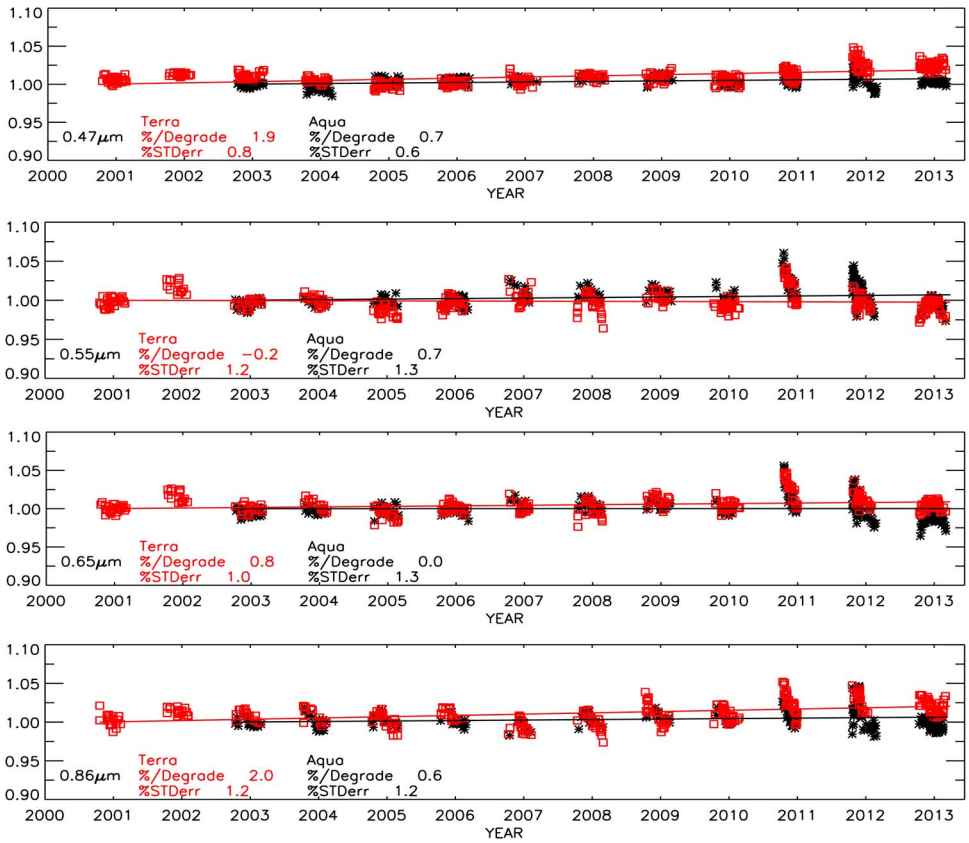

Fig. 2. Same as Fig. 1, but for Dome-C.

However, each invariant Earth target provides unique band-specific temporal trending. No consistent statement regarding single band trending can be made using all three invariant Earth targets. This indicates that the natural temporal oscillations of the invariant targets and methodology may be aliasing into the stability results. Bhatt *et al.* [19] found that if the trend over a decade exceeded the monthly standard error, the trend was significant. The significance tests were based on Weatherhead *et al.* [20], which accounted for both the natural variability and measurement autocorrelation of the invariant targets. For Terra, the 0.86-μm Dome-C trend is significant, but is not substantiated by Libya-4. Similarly, the Terra 0.47-μm Dome-C and DCC trends are significant but not supported by Libya-4. For Aqua, the 0.65- and 0.86-μm Libya-4 and DCC trends are meaningful, but are not verified by Dome-C. However, the stability based on all invariant targets for most VIS bands was within 1% for both Terra and Aqua C6 radiances. The Terra C6 calibration is an improvement over C5; however, for Aqua, the C6 calibration is comparable with C5.

III. Terra to Aqua Radiometric Scaling

A. NSNO Nadir Approach

The most straightforward approach to radiometrically scale one sensor to another is to use coincident bore-sighted, or ray-matched, radiance pairs. Given that even the best calibrated sensors are not perfectly stable and will drift over time, they must be scaled over the entire time period for when the two radiance records overlap. The 14 daily Terra and Aqua daytime ground track intersects occur at $\sim$68.3° latitude at approximately local noon. Unfortunately, intersects with SZAs less than 70° are only possible between March and September, limiting the temporal scaling record to six months out of year. In addition, the lowest SZA attainable at this latitude during summer solstice is 45°, thereby preventing the radiance pair comparisons over the entire range of Earth view radiances. The Terra and Aqua ground track intersects are not coincident, but are consistently $\sim$15 min apart. For this reason, this method is referred to as the nearly simultaneous nadir overpass (NSNO) technique.

Owing to the 15-min time difference, most of the Terra and Aqua radiance comparisons to date involve a transfer sensor [21], [22]. A transfer sensor provides coincident measurements, which may be necessary when comparing IR channels to mitigate differences in solar heating [23], [24]. For visible channels, the 15-min difference can be accounted for by averaging pixel-level radiances into 50-km regions. The 50-km regions mitigate the displacement of cloud and surface features owed to advection and imperfections in navigation. Wielicki *et al.* [25] examined the sensitivity of spatial matching noise to field-of-view (FOV) size in satellite intercalibration using NOAA-17 and NOAA-18 AVHRR SNO 0.65-μm radiance pairs and found that a 50-km averaging region reduces the noise by a factor of 2.5 when compared with a 12.5-km region. Reducing the time mismatch from 12 to 1.5 min decreases the noise by a factor of 1.4 over a large region, suggesting that time mismatches can be

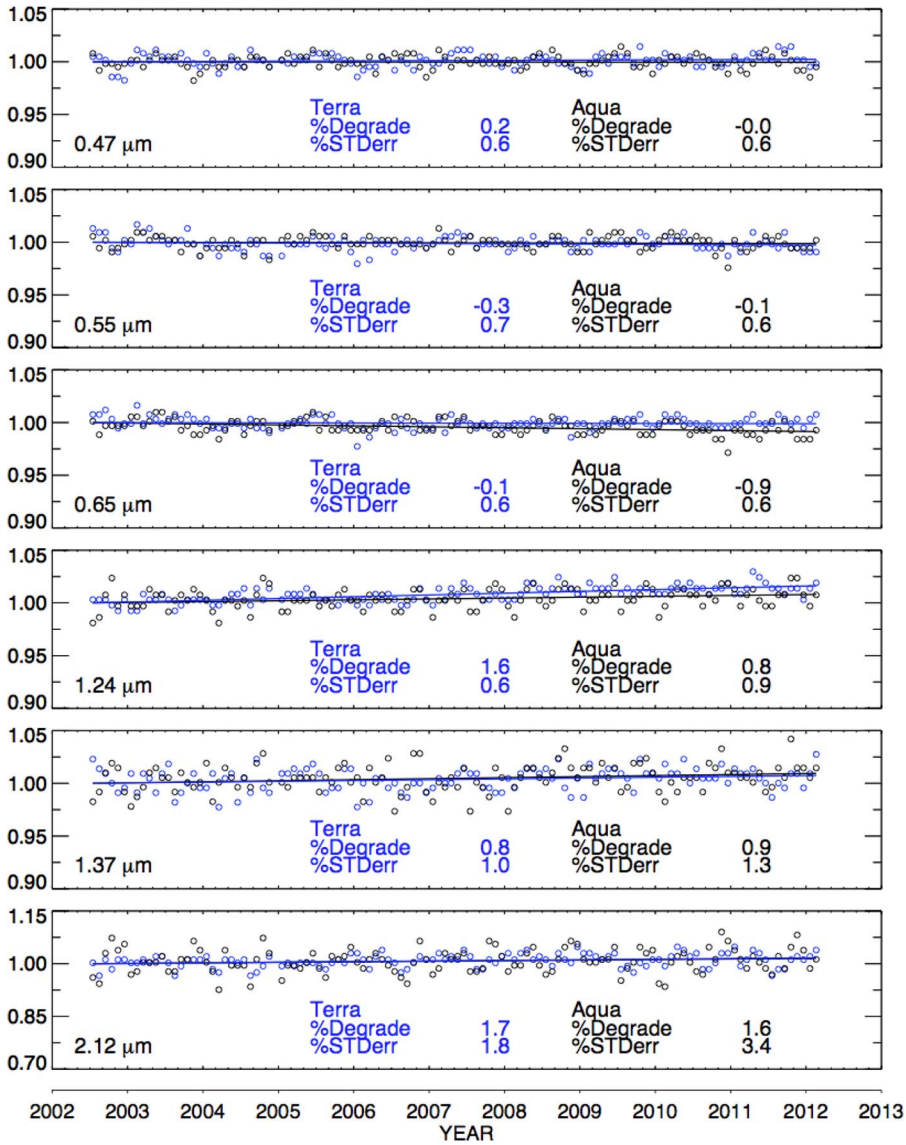

Fig. 3. Same as Fig. 1, but for DCC. The DCC data begin after July 2002 to avoid the poor data quality between 2000 and 2001.

mitigated using large FOVs. The 50-km NSNO radiance pairs are then normalized by the cosine of the SZA ($\mu 0$). This NSNO method has been successfully demonstrated in Minnis *et al.* [26].

B. NSNO Off-Nadir Approach

Two NSNO radiance pair methods are employed in this study. The first method only uses nadir measurements, and the second method uses off-nadir radiance pairs, as shown in Fig. 4. The off-nadir radiance pairs shown in Fig. 4 as open circles have identical view zenith angles, and the azimuthal angles are similar for view angles within 7.5°, given that the Terra and Aqua ground tracks intersect at local noon. Along the line of Terra and Aqua matched view angles, 1-km pixel-level radiances are averaged within 50-km-diameter FOVs. The 50-km FOVs are spaced along the line of matching view angles so that there is no overlap, both along the north-south and east-west axes (see Fig. 4). The advantage of the off-nadir method is that the frequency of 50-km radiance pairs is greatly increased

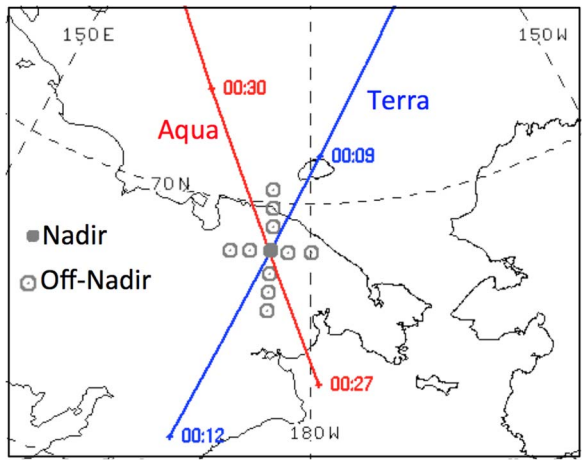

Fig. 4. Schematic of the (blue line) Terra and (red line) Aqua ground track intersect for June 9, 2010. The orbit time in GMT is labeled along the individual orbits. The nadir 50-km-diameter FOV is shown as the filled circle, and the off-nadir 50-km FOVs are shown as open circles.

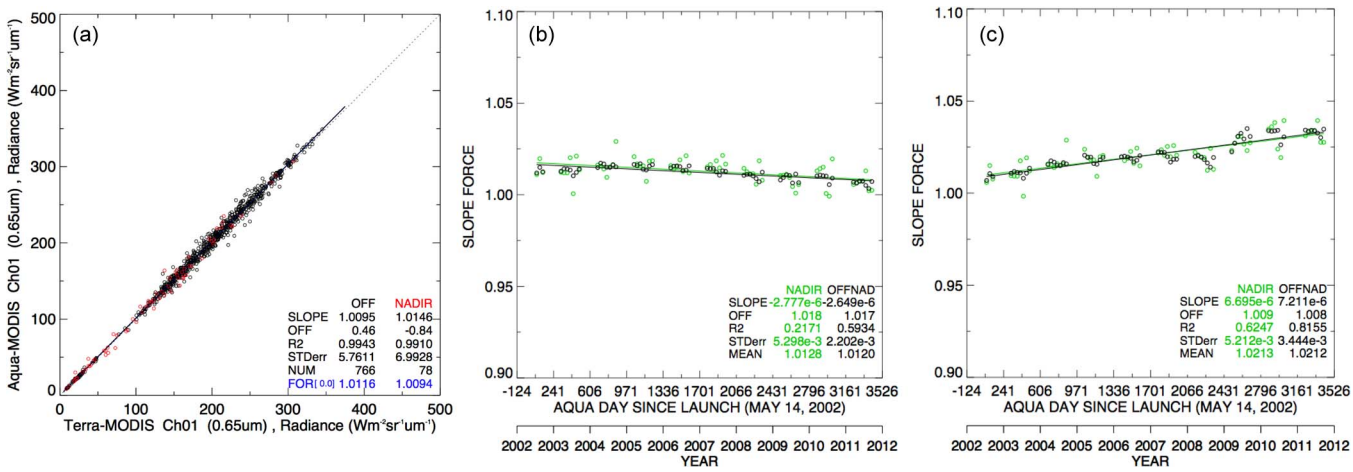

Fig. 5. (a) Scatterplot of the Terra- and Aqua-MODIS C6 NSNO (red points) nadir-only and (black points) off-nadir radiance pairs and (solid black) off-nadir linear regression line for July 2002. The dotted black line represents the perfect fit. (b) Monthly force fit slopes for both (green circles) nadir-only and (black circles) off-nadir, and corresponding temporal linear regressions with associated statistics are in the lower right. The slope and offset as defined in (1) are also given. (c) Same as (b), but for C5.

and the dynamic range is extended, given that the SZA is a function of latitude. The off-nadir approach has been successfully used to intercalibrate AVHRR visible radiances between NOAA morning and afternoon orbits [27] and to intercalibrate Aqua-MODIS (afternoon orbit) and NOAA-17 (morning orbit) AVHRR visible radiances [28]. Caution is required when using the off-nadir approach, since azimuthal mismatches may cause radiance pair biases. The off-nadir approach is first validated against the nadir-only approach.

Fig. 5(a) displays both the nadir-only and off-nadir Terra- and Aqua-MODIS band 1 0.65-μm radiance pairs observed during July 2002. The off-nadir matched radiance pairs are about ten times more than the nadir radiance pairs. Two least square linear regressions are applied to the radiance pairs. The first estimates the offset, whereas the second forces the offset through the origin. The off-nadir and nadir-only slopes are within 0.3% for both regressions. The off-nadir offset is 0.46 and is closer to the origin than the nadir-only offset of -0.84. The standard error of the regression is also smaller using the off-nadir radiance pairs.

The monthly force fit slopes for both nadir and off-nadir Terra- and Aqua-MODIS C6 band 1 (0.65 μm) radiance pairs are displayed in Fig. 5(b) and represent the Terra to Aqua monthly scaling factors. A linear regression of the monthly slopes captures most of the monthly slope variability. The temporal standard errors are 0.53% and 0.22% for the nadir-only and off-nadir force fit slopes, respectively. This suggests that the off-nadir NSNO method has reduced the ray-matching noise by more than one half when compared with the nadir-only method. The ten-year means of the monthly scaling factors are 1.0128 and 1.0120 for nadir-only and off-nadir, respectively. The mean scaling factors are consistent within 0.08%, indicating that the off-nadir slope replicates the nadir-only slope. The trend of the monthly slopes, or the relative C6 calibration, between Aqua and Terra appears to be stable between 2002 and 2008, where the Aqua radiance is $\sim$1.5% greater than Terra, after which the difference is reduced by half by the end of 2011. This is consistent with the Terra and Aqua VIS band divergence after 2007, where the Terra radiances are increasing and the Aqua radiances are decreasing, as stated in the summary in Section II.

C. C6 Terra Scaling Factors

Table III contains the Terra scaling factors for the other MODIS bands. To easily facilitate the implementation of the Terra scaling factors, a linear temporal trend was chosen to model the Terra scaling factors. The linear trend may not capture all of the interannual slope variability, which may be instrument related. Fig. 5(c), which is based on C5, clearly shows the discontinuity due to the SD door malfunction in 2003 and the SD recalibration in 2009. Stepwise linear scaling factors or higher order polynomials would capture all of the monthly slope variability, but one must apply band temporal specific complex set of scaling factors. However, the linear fit captured most of the slope variability and assures that the long-term relative Terra and Aqua calibration difference has been removed. For band 1, the off-nadir standard error indicates that 95% of the monthly slopes are within $\pm$0.44% of the linear trend. It is unknown what contribution of the trend residual is due to the NSNO method, given that the monthly slope fluctuations are usually greater than the year-to-year fluctuations, particularly for the nadir method and for longer wavelengths. The C6 Terra-scaled radiance, i.e., T_{scaled}, is computed from the C6 Terra radiance, i.e., T, as

$$T_{\text{scaled}} = \text{T} * (\text{offset} + \text{slope} * \text{DSL}) \tag{1}$$

where DSL is the day since the Aqua launch on May 14, 2002, and the band-specific offset and slope are located in Table III. The offset and slope are based on the linear trend of the off-nadir monthly force fit slopes and are valid between July 2002 and September 2011. The off-nadir and nadir-only lifetime mean Terra scaling factors for all bands are within 0.1%, and the trend difference is within 0.4%, except for bands 7 and 26, where the nadir-only standard error exceeds 7% and 1%, respectively.

TABLE III
TERRA TO AQUA MODIS C6 BAND-SPECIFIC SLOPE AND OFFSET SCALING FACTORS APPLICABLE TO (1) AND ASSOCIATED MEAN LIFETIME, TREND, AND TREND STANDARD ERROR. THE AQUA DIVIDED BY TERRA BAND SOLAR IRRADIANCE ($E_{A/T}$) RATIO IS ALSO GIVEN

Band C6		Scaling factors		Mean		Trend Stderr (%)		Trend (%/decade)		$E_{A/T}$
µm	#	offset	slope	nadir	off	nadir	off	nadir	off	
0.47	**3**	0.995	-1.50e-6	0.991	0.992	0.53	0.41	-0.25	-0.55	1.0022
0.55	**4**	1.004	-1.17e-6	1.001	1.002	0.42	0.30	-0.05	-0.43	1.0001
0.65	**1**	1.017	-2.65e-6	1.013	1.012	0.53	0.22	-1.01	-0.97	1.0016
0.86	**2**	1.001	-3.96e-6	0.994	0.994	0.46	0.33	-1.71	-1.45	0.9991
1.24	**5**	0.972	-2.54e-6	0.967	0.968	0.66	0.39	-1.32	-0.93	1.0423
1.38	**26**	1.038	-9.96e-7	1.036	1.036	7.31	1.34	-1.18	-0.36	0.9987
2.11	**7**	0.996	0.79e-6	0.998	0.997	1.17	0.41	0.02	0.29	0.9950

TABLE IV
SAME AS TABLE III, BUT FOR MODIS C5

Band C5		Scaling factors		Mean		Trend Stderr (%)		Trend (%/decade)	
µm	#	offset	slope	nadir	off	nadir	off	nadir	off
0.47	**3**	0.989	1.67e-5	1.023	1.018	0.76	0.68	7.95	6.10
0.55	**4**	1.001	5.81e-6	1.012	1.012	0.50	0.44	2.15	2.12
0.65	**1**	1.008	7.21e-6	1.021	1.021	0.52	0.34	2.44	2.63
0.86	**2**	0.995	6.77e-6	1.008	1.007	0.53	0.44	2.16	2.47
1.24	**5**	0.973	-1.13e-6	0.970	0.971	0.64	0.41	-0.84	-0.41
1.38	**26**	1.038	5.43e-7	1.041	1.039	7.09	1.44	-1.39	0.20
2.11	**7**	0.996	1.79e-6	0.999	0.999	1.18	0.39	0.43	0.65

Measurements from MODIS are reflectance based. Visible reflectance, i.e., ρ, is converted to radiance, i.e., L, by

$$L = \frac{[E_{\text{sun}}\ \rho\ \mu_0]}{\pi\ d^2_{\text{earth\_sun}}} \tag{2}$$

where $d^2_{\text{earth\_sun}}$ is the normalized Earth–Sun distance, and μ_0 is the cosine of the SZA. E_{sun} is the solar irradiance, which is based on [29]–[31], for wavelengths between 0.4 and 0.8 μm, 0.8 and 1.1 μm, and wavelengths greater than 1.1 μm, respectively [32]. To radiometrically scale a Terra to an Aqua reflectance, the Aqua divided by Terra band solar irradiance ratio must be applied to (1). If the Terra and Aqua SRFs are exactly identical, then this ratio is equal to 1. However, the Terra and Aqua SRFs are slightly different. Table III contains the Aqua divided by Terra solar irradiance ratio, which was calculated by convolving the SRF with the MCST solar irradiance. Most of the ratios are within ± 1.0022, except bands 5 and 7. Bands 5, 7, and 26 also have significant thermal leak and crosstalk issues and may not be identical between Terra and Aqua.

D. C5 Terra Scaling Factors

Table IV lists the MODIS band scaling factors for the C5 calibration. The band 1 C5 monthly slopes reflect the early 2009 SD 0.94-μm calibration adjustment, which decreased the Terra relative calibration compared with Aqua [4]. The MODIS C6 VIS band recalibration has successfully reduced the monthly slope variability, the mean relative Terra and Aqua calibration difference, and the corresponding trend significantly. The 0.65-μm C6 ten-year mean calibration difference is 1.2%, which was a 0.9% reduction from the C5 calibration. The VIS C6 off-nadir slope trends are within 1% per decade, except for band 2. The C5 VIS slopes were all greater than 2% per decade, and band 3 was $\sim$6% per decade. Oddly, the C5 band 3 (0.47 μm) nadir-only and off-nadir trends diverge over time (not shown). No other band exhibits this trait. During the first four years, the trends were comparable. Then, during 2011, the trends diverged by 2%. The C6 band 3 nadir-only and off-nadir trends are indistinguishable. The off-nadir points encompass multiple scan angle positions, whereas the nadir-only point is composed of a single scan angle. This verifies that the C6 calibration improved the temporal variation of the RVS dependence over the C5 calibration. Because the MODIS optics hardly degraded for SWIR bands and required very little

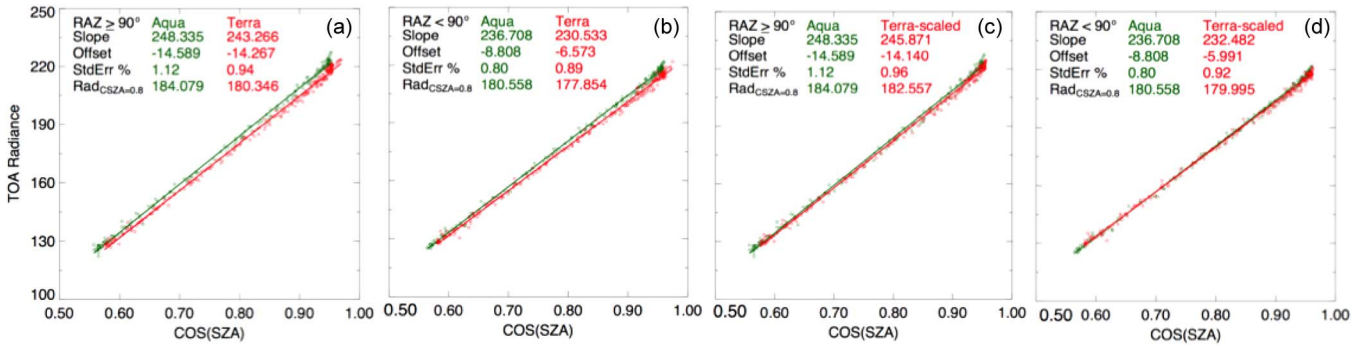

Fig. 6. (a) Libya-4 near-nadir TOA 0.65-μm radiances as a function of $\mu 0$ for Aqua (green) and Terra C6 (red) with associated linear regression and statistics in the upper left for backscatter conditions. (b) Same as (a), but for forward scatter conditions. (c) Same as (a), but for Terra-scaled. (d) Same as (c), but for forward scatter conditions.

calibration adjustments, the C5 and C6 scaling factors and statistics are similar. In order to scale Terra C5 to Aqua, the scaling factors in Table IV should be applied to (1).

IV. Invariant Target Validation of Scaling Factors

The NSNO approach radiometrically scales the Terra radiances to Aqua. The Terra scaling factors are validated using both invariant targets (see Section IV) and transfer radiometers (see Section V). Consistency in the scaling factors between these independent approaches validates the accuracy of the scaling factors and also assures that the scaling factors are viable for many applications.

A. Libya-4 Desert

A common way to characterize the Libya-4 reflectance is to model the clear-sky near-nadir radiance or reflectance multiplied by $\mu 0$ as a function of SZA [33]. This type of model works best if both the Libya-4 and MODIS reflectances are temporally stable. As discussed in Section II, the Terra and Aqua visible bands are stable based on Libya-4 within 1% and 1.8% per decade, respectively. Bhatt *et al.* [34] [see Fig. 1(b)] found that the Aqua-MODIS 0.65-μm observed Libya-4 radiances were stratified by scattering direction, for $\mu 0$ greater than 0.6. The forward minus backscatter ten-year mean radiance difference was +0.9%. The ten-year linear trend standard errors of Aqua-MODIS near-nadir radiances as a function of $\mu 0$ were 1.5%, 1.1%, and 0.8% for the combined, backscatter, and forward scatter conditions, respectively. Examining the forward and backscatter conditions separately increases the confidence of comparing Terra- and Aqua-MODIS radiances using a desert target over all scattering conditions.

Fig. 6 shows the Terra, Terra-scaled, and Aqua C6 TOA 0.65-μm near-nadir (view angles within 10°) 50 × 50 km spatial gridded instantaneous clear-sky radiances over Libya-4 as a function of $\mu 0$ in the forward direction and backscatter conditions. A spatial uniformity threshold of the pixel-level reflectances is used to determine clear-sky conditions. The radiances are linearly regressed with respect to $\mu 0$, and the resulting slope, offset, and standard error are also given. It is evident in Fig. 6 that the Terra-scaled radiances more closely resemble the Aqua radiances in both forward and backscatter conditions. In order to quantify the accuracy of the Terra scaling factors, the Terra minus Aqua radiance difference at 0.8 $\mu 0$ is computed. The Terra minus Aqua forward and backscatter radiance difference is −1.5% and −2.0%, respectively; whereas the Terra-scaled one is −0.3% and −0.8%, respectively. As expected, the Terra scaling factors increased the Terra radiance by 1.2% for both backscatter and forward scatter conditions. Although the Terra-scaled minus Aqua radiance differences are not exactly zero, they are closer than the Terra C6 radiances and are within the overall standard error of 1.1%.

Table V contains the ten-year Terra minus Aqua relative calibration difference for both forward and backscatter conditions, and Table VI provides the associated trend standard error. The Libya-4 radiance was too dark in the 1.38 μm to quantify the scaling factor improvement. The 1.24-μm band radiance required a thermal leak correction, which ranges between 0.5% and 3.0% for cold and hot targets, respectively. The NSNO occurs at 68.3° N latitude, having much colder conditions than over the hot Libyan Desert, the latter of which may not capture the thermal leak contribution.

For the 0.86- and 0.47-μm bands, the scaling factors enlarged the relative calibration difference. For the VIS bands, the Terra-scaled minus Aqua difference is always negative. Perhaps the Libya-4 reflectance is brighter in the afternoon during the Aqua overpass time than in the morning for the same $\mu 0$ owing to the sand dune orientation affecting illumination. The calibration difference is greater in backscatter than in forward scatter conditions by ∼0.5%, suggesting that the Libya-4 anisotropic effects are not being accounted for. The Aqua standard error is much greater for backscatter than forward scatter conditions, whereas for Terra, they are similar, which may indicate a greater aerosol activity during Aqua overpass times. However, only the 0.47-μm band, where the aerosol impact is the greatest, did the backscatter calibration difference exceeded the trend standard error for the VIS bands.

B. Dome-C

Fig. 7 shows the Terra, Terra-scaled, and Aqua C6 0.65-μm TOA observed radiances as a function of $\mu 0$ over Dome-C using

TABLE V
TERRA (C6) AND TERRA-SCALED (SCALED) MINUS AQUA MODIS MEAN BAND RADIANCE (%) BETWEEN 2002 AND 2012 FOR LIBYA-4, DOME-C, AND DCC. FOR LIBYA-4, THE MEAN RADIANCE IS STRATIFIED BY THE FORWARD (FOR) AND BACK (BACK) SCATTER DIRECTIONS

MODIS Band		Libya-4				Dome-C		DCC	
		Terra-C6		Terra-scaled					
µm	#	For	Back	For	Back	C6	scaled	C6	scaled
0.47	**3**	-0.3	-1.0	-1.1	-1.8	0.6	-0.2	1.1	0.2
0.55	**4**	-0.5	-1.3	-0.3	-1.1	-0.1	0.0	0.0	0.1
0.65	**1**	-1.5	-2.0	-0.3	-0.8	-1.1	0.0	-1.0	0.2
0.86	**2**	-0.2	-0.6	-0.8	-1.2	0.4	-0.3		
1.24	**5**	1.2	0.8	-2.0	-2.3			5.1	1.6
1.38	**26**							0.9	4.6
2.12	**7**	0.4	-0.4	0.0	-0.8			-5.0	-5.0

TABLE VI
TERRA- AND AQUA-MODIS C6 BAND TREND STANDARD ERROR IN PERCENT FOR LIBYA-4, DOME-C, AND DCC

MODIS Band		Libya-4				Dome-C		DCC	
		Forward		Back					
µm	#	Terra	Aqua	Terra	Aqua	Terra	Aqua	Terra	Aqua
0.47	**3**	1.2	1.0	1.0	1.1	0.6	0.5	0.6	0.6
0.55	**4**	0.9	1.0	0.9	1.2	1.7	1.5	0.7	0.6
0.65	**1**	0.9	0.8	0.9	1.1	1.5	1.3	0.6	0.6
0.86	**2**	0.9	0.8	1.0	1.1	1.5	1.4		
1.24	**5**	1.2	1.1	1.2	1.1			0.6	0.9
1.38	**26**							1.0	1.3
2.12	**7**	2.2	2.0	2.4	2.2			1.8	3.4

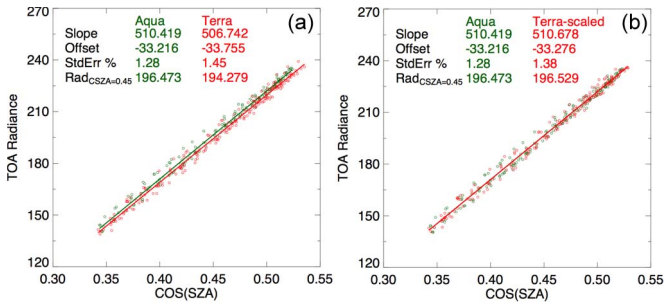

Fig. 7. (a) Dome-C near-nadir TOA 0.65-μm radiances as a function of $\mu 0$ for Aqua (green) and Terra C6 (red) with associated linear regression and statistics in the upper left. (b) Same as (a), but for Terra-scaled.

the same Libya-4 procedure, except in this case, no forward and backscatter dependence was observed. For Dome-C, the Terra minus Aqua radiance difference is considered at a $\mu 0$ of 0.45. For the SWIR bands, the signal-to-noise ratio was insufficient to validate the scaling, being that the trend standard error was in the 6%–20% range. For the VIS bands, the NSNO Terra scaling factors reduced the calibration difference from within 1.1%–0.3%. Unlike Libya-4, the NSNO Terra scaling factors are consistent with Dome-C.

C. DCC

The same DCC procedure used to determine temporal trending is used to determine the consistency between the Terra and Aqua C6 calibration, except that the DCC overhead reflectances are not normalized. Fig. 8 displays the Terra-scaled, Terra C6, and Aqua C6 DCC reflectances over time. The Terra-scaled one resembles the Aqua 0.65-μm DCC reflectance for both the lifetime mean reflectance and degradation. Table VI indicates that the DCC Terra minus Aqua 0.65-μm difference is -1% for the C6 calibration and 0.2% for Terra-scaled. As anticipated, the Terra scaling factors increased the Terra calibration by 1.2%. In fact, for all VIS bands, the difference is within 0.2%, thereby validating the NSNO scaling factors. DCC provide the lowest standard errors of all the invariant targets because they have the greatest signal-to-noise ratio and are the most isotropic.

For the SWIR bands, which are impacted by thermal leak and crosstalk issues, the thermal leak correction for DCC is minimal given that DCC pixels are identified with cloud top temperatures that are less than 205°K. The NSNO scaling factors had a greater thermal leak correction. Over Libya-4, where the thermal leak correction is greatest, the Terra scaling factors are more consistent with NSNO than with DCC. For

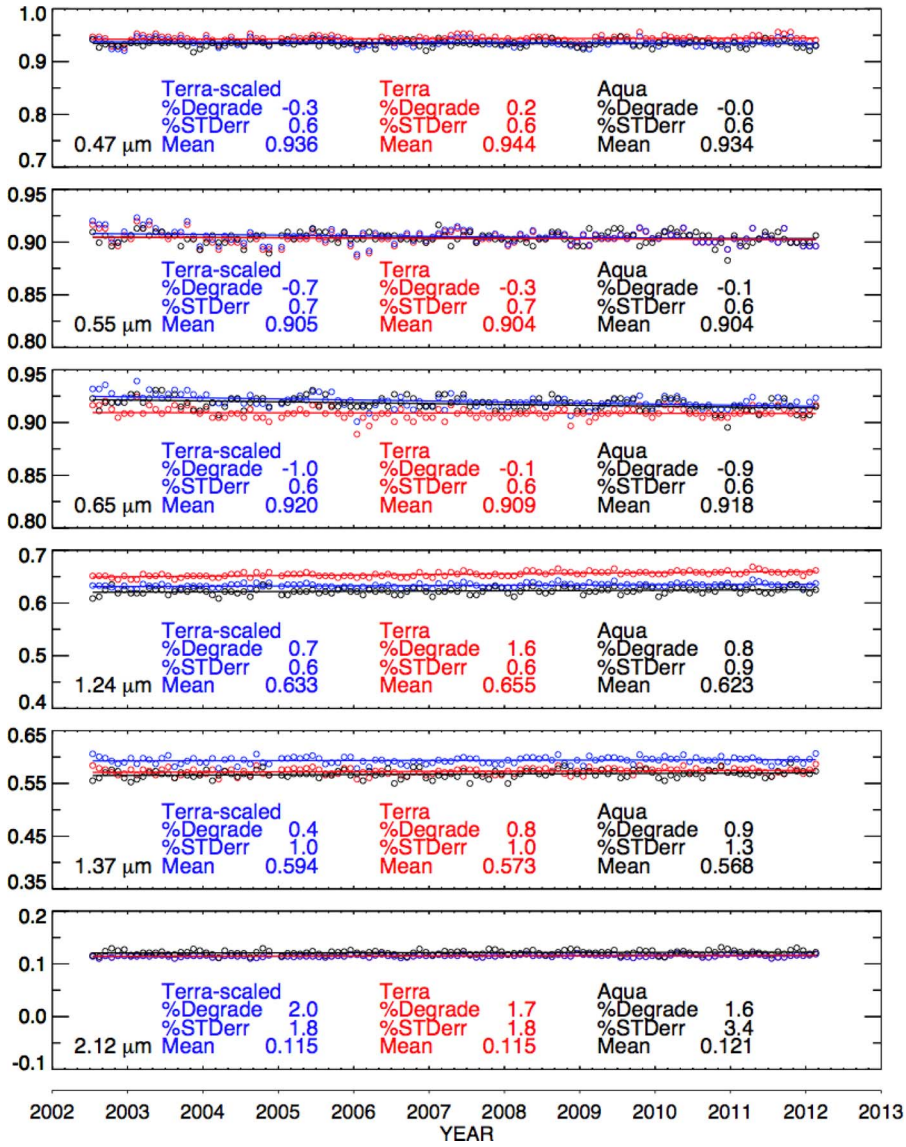

Fig. 8. (a) Terra-scaled (blue), Terra C6 (red), and Aqua (black) DCC TOA monthly reflectances and temporal trend lines and corresponding statistics.

the SWIR bands, the radiances are also affected by ice crystal microphysics, which vary during the DCC life cycle. Because the DCC are sampled over the entire tropical zone, including over land, systematic ice crystal habit differences may occur between Terra and Aqua overpass times.

V. GEO Intercalibration Validation of Scaling Factors

In this paper, multiple GEO satellite imagers operating during the MODIS record will be used as transfer radiometers to verify the Terra scaling coefficients in Section III. The Terra scaling factors are validated if the GEO intercalibration gain derived from the Terra-scaled radiances is more consistent with that from the Aqua radiances, than from the Terra radiances. The Meteosat-8 and Meteosat-9 imagers were demonstrated as effective transfer radiometers to evaluate the Terra and Aqua calibration difference [35], [36]. The advantage of ray matching over an invariant target approach is that the ray matching provides radiance pairs over the entire range of Earth-reflected radiances on a monthly basis. The Clouds and the Earth's Radiant Energy System (CERES) [37] project employs GEO/MODIS ray-matched coincident radiance pairs to tie the calibration to MODIS in order to derive consistent cloud and radiative property retrievals between successive GEO satellites and between GEO domains [38], [39]. All GEO visible sensors to date lack onboard calibration. If Terra and Aqua MODIS instruments are radiometrically scaled, then each MODIS instrument provides an independent calibration transfer.

This study follows the CERES GEO/MODIS ray-matching approach in Morstad *et al.* [39] and Doelling *et al.* [40]. Over the GEO equatorial domain, the GEO imager pixel level counts, which are proportional to radiance, and MODIS radiances are averaged onto a 0.5° longitude by 0.5° latitude grid, provided the measurements are coincident within 15 min. The GEO domain encompasses ±20° E/W and ±15° N/S from the GEO subsatellite location. Because land regions have unique spectral signatures, only all-sky ocean regions are considered in order

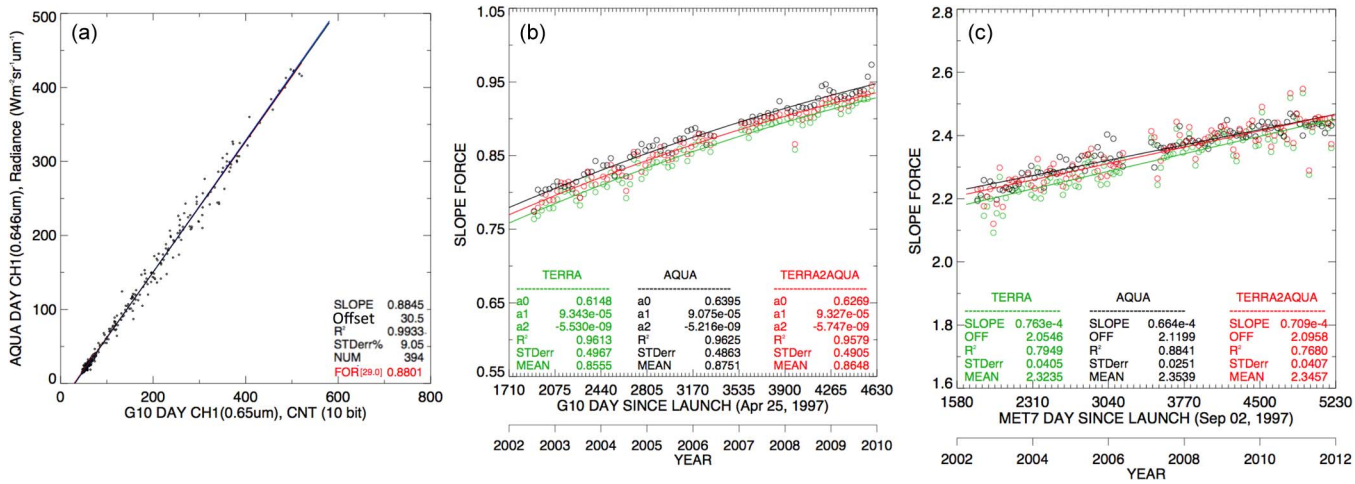

Fig. 9. (a) Scatterplot of coincident ray-matched Aqua-MODIS band 1 (0.65 μm) normalized radiance and the GOES-10 count pairs during October 2008. The (black line) least squares and (red line) force fit regression lines through the GOES-10 space count of 29 are also shown. The Offset statistic term is the x-axis offset. (b) GOES-10 monthly gains based on Terra (green), Aqua (black), Terra-scaled (red), and associated second-order temporal fit. The GOES-10 eight-year record gain coefficients (a0,a1,a2), correlation coefficient (r2), standard error of the quadratic fit (STDerr), and mean record gain (MEAN) are given at the bottom of the plot. (c) Same as (b), but for Meteosat-7 and corresponding linear trend.

to diminish the impact of the radiance contribution not shared by both spectral band response functions. The same spectral band adjustment factor (SBAF) is applied to both the Terra- and Aqua-MODIS radiances to make them spectrally equivalent to the GEO radiance. The SBAF is based on the Environmental Satellite (Envisat)-SCanning Imaging Absorption SpectroMeter for Atmospheric CHartographY (SCIAMACHY) hyperspectral radiances [41]–[43]. Only the nonsunglint angular matched radiances within 15° for both viewing and relative azimuthal angles are paired. The radiance pairs are normalized with respect to the cosine of the SZA. The GEO calibration gain, i.e., g, is computed by

$$R_{\text{modis}} * \text{SBAF}_{\text{geo/aqua}} * \left(\frac{\mu_{0\text{geo}}}{\mu_{0\text{modis}}}\right) = g * (C - C_0) \quad (3)$$

where R_{modis} is the MODIS radiance in $\text{W} \cdot \text{m}^{-2} \cdot \text{sr}^{-1} \cdot \mu\text{m}^1$; μ_0 is the cosine of the SZA; and C and C_0 are the GEO observed count and published space count, respectively. $\text{SBAF}_{\text{geo/aqua}}$ is the spectral correction applied to the MODIS radiance needed to provide a GEO equivalent radiance.

Fig. 9(a) displays the Aqua-MODIS band 1 (0.65 μm) normalized [left side of (3)] radiance and the Geostationary Operational Environmental Satellite (GOES) 10 count pairs during October 2008. A least-squares regression and a force fit slope anchored to the GEO published space count are computed. If the ray-matching algorithm were perfect, then the least squares and force fit slopes should be identical. For this month, the slopes are within 0.5%, and the least squares offset of 30.5 is close to the GOES-10 published offset of 29 counts. Fig. 9(b) presents the force fit gains based on Aqua, Terra, and Terra-scaled radiances between 2002 and 2010. The data gap in 2006 denotes the time when GOES-10 was moved from the GOES-East position (75° W) to the South American location (59.6° W). A second-order temporal fit best describes the GOES-10 degradation. The temporal fits based on the MODIS gains are nearly parallel, confirming the consistent stability between the Terra and Aqua C6 calibrations, where the GOES-10 eight-year mean gains based on Aqua, Terra-scaled, and Terra were 0.875, 0.865, and 0.856, respectively [see Fig. 8(b) statistics from the bottom of the plot]. Although the Terra scaling factors increased the GOES-10 gain by 1%, the Terra-scaled based gain is still short of the Aqua-based gain by 1.1%. Fig. 9(c) shows the Meteosat-7 12-year mean gains based on Terra, Terra-scaled, and Aqua MODIS C6 radiances. The Terra minus Aqua and Terra-scaled minus Aqua based Meteosat-7 gains are -1.3% and -0.3%, respectively. In this case, the Terra-scaled Meteosat-7 gain is within -0.3% of the Aqua Meteosat-7 gain and is nearly parallel over time. The Meteosat-7 gain is a factor of 4 greater than the GOES-10 gain, since the Meteosat-7 and GOES-10 gains have 8-bit and 10-bit count resolutions, respectively.

If the GEO and MODIS SRFs were identical and the underlying radiance field was invariant between the Terra 10:30 A.M. local equator crossing time (LECT) and Aqua 1:30 P.M. LECT overpass times, then only the Terra and Aqua calibration difference would be observed. However, this is not the case when using GEOs as transfer radiometers. Fig. 10(a) shows the spectral band differences among the MODIS band 1, GOES-10 VIS, and Meteosat-7 VIS channels. The Meteosat-7 bandwidth is much larger and centered more toward 0.75 μm and contains NIR water vapor absorption bands, which are not seen by the other two instruments. In addition to the humidity conditions between Terra and Aqua overpass times, the cloudy and clear conditions over the ray-matching domain can vary diurnally (e.g., maritime stratus clouds, whose spatial extent is seasonally dependent). The greater the difference in the trend standard errors between Terra and Aqua, as listed in Table VII, the greater the change of cloud and humidity conditions between overpass times.

The cloud type, opaqueness, and height differences will modify the SBAF, for which the magnitude is dependent on the unshared portion of the SRF radiance contribution. The brighter the clouds and the greater the SRF similarity, the smaller the SBAF uncertainty will be. The SBAF is computed

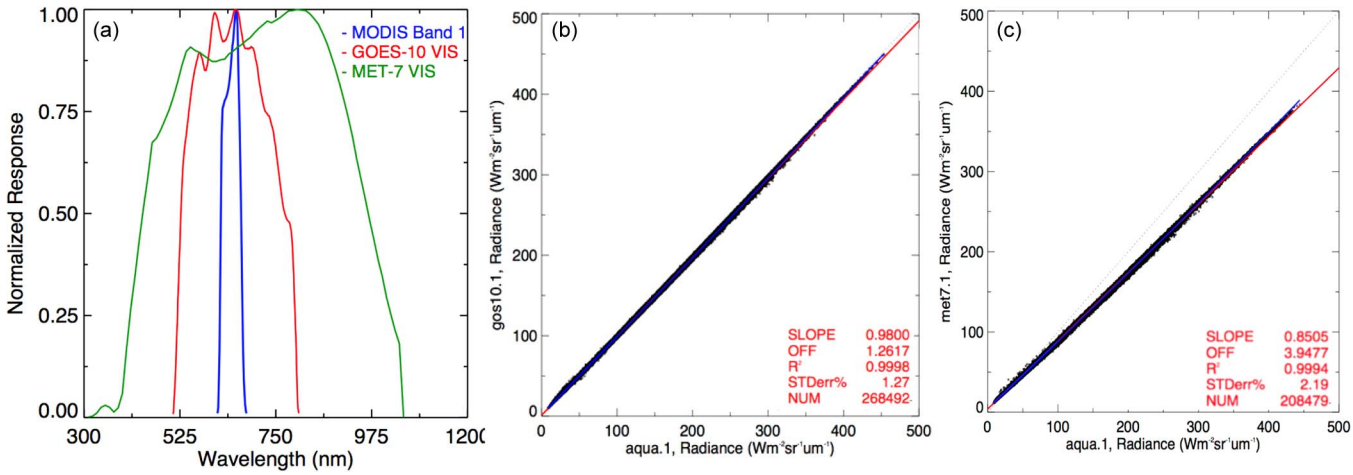

Fig. 10. (a) Normalized 0.65-μm band SRFs of Aqua-MODIS, GOES-10, and Meteosat-7. (b) Scatterplot of GOES-10 visible and Aqua-MODIS 0.65-μm SRF convolved SCIAMACHY pseudo radiance pairs during 2002–2010 over the GOES-10 equatorial domain. The red line represents the linear regression, and the associated statistics are in the lower right corner. The blue line represents the quadratic fit, which is used to define the SBAF in this paper. (c) Same as (b), but for Meteosat-7 visible and Aqua-MODIS 0.65 μm.

TABLE VII
GEO BEGINNING AND END OF RECORD, SUBSATELLITE LONGITUDE, SBAF UNCERTAINTY, TERRA (C6) AND TERRA-SCALED (SCALED) MINUS AQUA MODIS MEAN RECORD BAND GAIN DIFFERENCE, AND ASSOCIATED MONTHLY GAIN STANDARD ERROR

Satellite	GEO Record		GEO longitude	SBAF (%)	Terra-Aqua mean gain (%)		Trend stderr(%)	
	Start	End			C6	Scaled	Terra	Aqua
GOES-9	Apr 2003	Oct 2005	155°E	1.1	-1.7	-0.5	0.5	0.5
GOES-10*	Jul 2002	Dec 2009	135°/60° W	1.3	-2.2	-1.2	0.5	0.5
GOES-11	Jul 2006	Dec 2011	135°W	1.4	-2.3	-1.5	1.2	0.8
GOES-12°	Apr 2003	Dec 2011	75°/60°W	1.2	-1.5	-0.6	0.5	0.5
GOES-13	Apr 2010	Dec 2011	75°W	0.8	-0.9	-0.2	0.2	0.6
Meteosat-5	Jul 2002	Jan 2007	63°E	2.1	-0.3	+0.9	5.2	2.2
Meteosat-7#	Jul 2002	Dec 2011	0°/57°E	2.1	-1.3	-0.3	4.1	2.5
Meteosat-8	May 2004	Mar 2007	3°W	0.3	-1.4	-0.2	0.4	0.6
Meteosat-9	Apr 2007	Dec 2011	0° E	0.3	-0.4	+0.3	0.3	0.5

* GOES-10 Includes South American coverage beginning in Dec. 2006

° GOES-12 Includes South American coverage beginning in May 2010

Meteosat-7 Includes the Indian Ocean coverage beginning in Feb. 2007

by regressing the SCIAMACHY hyperspectral convolved with MODIS and GOES SRF footprint radiance pairs over the same GEO equatorial domain. The Envisat sun-synchronous satellite has an LECT of 10:00 A.M. Fig. 10(b) shows the linear regression of the SCIAMACHY pseudo MODIS and GOES-10 radiance pairs, where the corresponding standard error or the SBAF uncertainty is 1.3%. For comparison, the Meteosat-7 and MODIS pseudo radiance pairs are given in Fig. 10(c). Because the Meteosat-7 SRF is nearly broadband, it has an associated standard error of 2.1%. The GEO SBAF uncertainties are listed in Table VII.

Table VII reveals that, overall, the nine-satellite mean Terra and Terra-scaled minus Aqua based GEO gain difference is −1.3% and −0.4%, respectively. This result validates that the Terra-scaled radiances are more closely radiometrically scaled to Aqua than those of Terra. In addition, the mean difference of −1.3% between the Terra- and Aqua-based GEO gains closely matches with the off-nadir mean lifetime C6 scaling factor (1.012) of the 0.65-μm band in Table III. The GEO satellites with the least diurnal impact, defined as those with SBAF uncertainties less than 1%, have Terra-scaled minus Aqua based GEO gain differences within 0.3%. The GEO satellites with

the greatest diurnal influence, which have large Terra and Aqua trend standard error differences and SBAF uncertainties greater than 2%, have gain differences within 0.9%. These differences are well within the trend and SBAF uncertainty. The remaining GEOs all have negative gain differences. Only the two GEOs located at 135° W have gain differences much less than −0.6%. Here, the underlying cause may be the lack of bright reflective intertropical convergence zone (ITCZ) cloud coverage, which has reduced the dynamic range of the radiance pairs.

VI. Conclusion

The MCST has recently released the MODIS C6 radiance product. C6 has removed all known calibration drifts by recalibrating the SD/SDSM, lunar, and RVS measurements for temporal stability. In general, the lifetime Terra or Aqua C6 stability is within 1% for most VIS bands based on the Libya-4 Desert, Dome-C, and DCC invariant targets. The Terra C5 wavelength-dependent degradation has been removed, particularly for the 0.44- and 0.47-μm bands, where the drifts exceeded 6%. In general, the Terra and Aqua C6 VIS bands diverge after 2007, where Aqua is degrading relative to Terra. The small band-specific C6 temporal calibration drifts based on Libya-4, Dome-C, and DCC are not consistent, suggesting that the limits of the invariant target calibration capability have been reached and are being aliased by the natural reflectance oscillations of the invariant targets and from methodology restraints. The invariant target trend standard errors range between 0.6% and 1.4% for most VIS bands.

The Terra- and Aqua-MODIS NSNO radiance pairs were used to radiometrically scale Terra to Aqua. The C6 calibration reduced both the relative Terra and Aqua calibration and lifetime trend differences. The mean C6 relative calibration and trend difference are within 1.2% and 1% per lifetime, whereas the C5 difference and trend were 2% and 2% per lifetime for most VIS bands. The Terra radiometrically scaled and Aqua calibration VIS differences are within 0.3% over Dome-C and DCC. DCC and Dome-C signatures are spectrally flat bright isotropic reflectors with minimal water vapor burden. Unlike Dome-C and DCC, the Libya-4 Terra-scaled and Aqua calibration differences are negative, but within the trend standard error, except for the 0.47-and 0.86-μm channels, for which the difference is increased over that for Terra C6. The Libya-4 results are less consistent due to unaccounted residual bidirectional effects between the Terra and Aqua overpass times. For GEO sensors with similar 0.65-μm SRFs as MODIS, the Terra-scaled and Aqua relative calibration is within 0.3%. For most GEO sensors, the relative Terra-scaled calibration is within 0.6% and is more consistent than the Terra C6 calibration.

For SWIR bands, the C6 calibration only results in minor adjustments to the C5 calibration. The Terra and Aqua relative calibration difference is mainly based on the characterization of the absolute calibration and changes encountered during the transfer to orbit. These bands experience thermal leaks and electronic crosstalk, causing inconsistent Libya-4 and DCC radiometric scaling results. The DCC radiances are a function of their lifecycle—owed to changing ice crystal physics—and may not be consistent during Terra and Aqua overpass times, particularly over land. Based on these conclusions, the Terra scaling factors are not robust for wavelengths greater than 1 μm.

The Terra scaling factors may be dependent on the underlying scene, which are defined by the surface and cloud conditions. DCC and Dome-C provide consistent scaling factors, whereas tropical desert and GEO/MODIS intercalibration suggests slightly greater scaling factors. Scene and diurnal differences are difficult to discern. Comparing Aqua-MODIS and NPP-VIIRS SNO radiance pairs, which have almost identical spectral bands and LECT, over several scene types will provide further insight [44]. In addition, current invariant Earth target approaches have an overall calibration transfer uncertainty of ∼1%, implying that any greater accuracy in radiometric scaling will be difficult. The future well-calibrated hyperspectral Climate Absolute Radiance and Refractivity Observatory sensor [45], onboard a precessionary spacecraft, will be able to distinguish sensor calibration differences from a wide variety of planetary scene conditions and diurnal cycles, thereby offering improvements in radiometric scaling of historical sensors.

Acknowledgment

The GEO satellite data were obtained from the University of Wisconsin Space Science and Engineering Center, Madison, WI, USA. The authors would like to thank the GSICS Research Working Group for all the insightful discussions.

References

[1] V. V. Salomonson, W. L. Barnes, P. W. Maymon, H. E. Montgomery, and H. Ostrow, "MODIS: Advanced facility instrument for studies of the Earth as a system," *IEEE Trans. Geosci. Remote Sens.*, vol. 27, no. 2, pp. 145–153, Mar. 1989.

[2] W. L. Barnes, X. Xiong, and V. V. Salomonson, "Status of Terra MODIS and Aqua MODIS," *Adv. Space Res.*, vol. 32, no. 11, pp. 2099–2106, Dec. 2003.

[3] X. Xiong and W. L. Barnes, "An overview of MODIS radiometric calibration and characterization," *Adv. Atmos. Sci.*, vol. 23, no. 1, pp. 69–79, Jan. 2006.

[4] A. Wu *et al.*, "Characterization of Terra and Aqua MODIS VIS, NIR, and SWIR spectral band calibration stability," *IEEE Trans. Geosci. Remote Sens.*, vol. 51, no. 7, pp. 4330–4338, Jul. 2013.

[5] X. Xiong, J. Sun, X. Xiaobo, W. Barnes, and V. Salomonson, "On-orbit calibration and performance of Aqua MODIS reflective solar bands," *IEEE. Trans. Geosci. Remote Sens.*, vol. 48, no. 1, pp. 535–546, Jan. 2010.

[6] X. Xiong, J. Sun, and W. Barnes, "Intercomparison of on-orbit calibration consistency between Terra and Aqua MODIS reflective solar bands using the Moon," *IEEE. Trans. Geosci. Remote Sens. Lett.*, vol. 5, no. 4, pp. 778–782, Oct. 2008.

[7] J. Sun, X. Xiong, and W. Barnes, "MODIS reflective solar bands on-orbit calibration using the moon," *IEEE Trans. Geosci. Remote Sens.*, vol. 45, no. 7, pp. 2383–2393, Jul. 2007.

[8] X. Xiong, N. Che, and W. Barnes, "Terra MODIS on-orbit spectral characterization and performance," *IEEE Trans. Geosci. Remote Sens.*, vol. 44, no. 8, pp. 2198–2206, Aug. 2006.

[9] J. Sun *et al.*, "On-orbit performance of the MODIS reflective solar bands time-dependent response versus scan angle algorithm," in *Proc. SPIE- Earth Observ. Syst. XVII*, 2012, vol. 8510, Art. ID. 85100J.

[10] J. Sun *et al.*, "MODIS RSB calibration improvements in Collection 6," in *Proc. SPIE*, 2012, vol. 8528, Art. ID. 85280N.

[11] G. Toller *et al.*, "Terra and Aqua MODIS collection 6 Level 1B algorithm," *J. Appl. Remote Sens.*, vol. 7, no. 1, May 2013, Art. ID. 073557.

[12] X. Xiong *et al.*, "Terra and Aqua MODIS calibration algorithms and uncertainty analysis," in *Proc. SPIE Sens., Syst., Next-Gener. Satellites IX*, 2005, vol. 5978, Art. ID. 59780V.

[13] M. Goldberg *et al.*, "The global space-based inter-calibration system," *Bull. Amer. Meteorol. Soc.*, vol. 92, no. 4, pp. 467–475, Apr. 2011.

[14] A. Wu, X. Xiong, C. Cao, and A. Angal, "Monitoring MODIS calibration stability of visible and near-IR bands from observed top-of-atmosphere BRDF-normalized reflectances over Libyan desert and Antarctic surfaces," in *Proc. SPIE Earth Observ. Syst. XIII*, 2008, vol. 7081, Art. ID. 708113.
[15] A. Angal, X. Xiong, T. Choi, G. Chander, and A. Wu, "Using the Sonoran and Libyan Desert Test Sites to monitor the temporal stability of reflective solar bands for Landsat 7 ETM+ and Terra MODIS sensors," *J. Appl. Remote Sens.*, vol. 4, no. 1, Apr. 2010, Art. ID. 043525.
[16] S. G. Warren, R. E. Brandt, and P. O'Rawe Hinton, "Effect of surface roughness on bidirectional reflectance of Antarctic snow," *J. Geophys. Res.*, vol. 103, no. E11, pp. 25 789–25 807, Oct. 1998.
[17] D. R. Doelling, D. Morstad, B. R. Scarino, R. Bhatt, and A. Gopalan, "The characterization of deep convective clouds as an invariant calibration target and as a visible calibration technique," *IEEE Trans. Geosci. Remote Sens.*, vol. 51, no. 3, pp. 1147–1159, Mar. 2013.
[18] N. G. Loeb *et al.*, "Angular distribution models for top-of-atmosphere radiative flux estimation from the Clouds and the Earth's Radiant Energy System instrument on the tropical rainfall measuring mission satellite. Part I: Methodology," *J. Appl. Meteorol.*, vol. 42, no. 2, pp. 240–265, Feb. 2003.
[19] R. Bhatt *et al.*, "Initial stability assessment of S-NPP VIIRS reflective solar band calibration using invariant desert and deep convective cloud targets," *Remote Sens.*, vol. 6, no. 4, pp. 2809–2826, Mar. 2014.
[20] E. C. Weatherhead *et al.*, "Detecting the recovery of total column ozone," *J. Geophys. Res.*, vol. 105, no. D17, pp. 22 201–22 210, Sep. 2000.
[21] A. Wu, X. Xiong, H. Murakami, and W. Barnes, "Inter-comparison of Aqua and Terra MODIS using Adeos-II GLI orbital intersections," in *Proc. SPIE*, 2005, vol. 5882, Art. ID. 58820X.
[22] X. Xiong, A. Wu, J. Sun, and B. Wenny, "An overview of intercomparison methodologies for Terra and Aqua MODIS calibration," in *Proc. SPIE*, 2006, vol. 6296, Art. ID. 62960C.
[23] L. Yonghong, A. Wu, and X. Xiong, "Evaluating calibration of MODIS thermal emissive bands using infrared atmospheric sounding interferometer measurements," in *Proc. SPIE*, 2013, vol. 8724, Art. ID. 87240X.
[24] A. Wu, C. Cao, and X. Xiong, "Intercomparison of the 11- and 12-μm bands of Terra and Aqua MODIS using NOAA-17 AVHRR," in *Proc. SPIE*, 2003, vol. 5151, pp. 384–394.
[25] B. A. Wielicki *et al.*, "Climate quality broadband and narrowband solar reflected radiance calibration between sensors in orbit," in *Proc. IEEE Int. Geosci. Remote Sens. Symp.*, 2008, pp. I-257–I-260.
[26] P. Minnis, D. R. Doelling, L. Nguyen, W. Miller, and V. Chakrapani, "Assessment of the visible channel calibrations of the TRMM VIRS and MODIS on Aqua and Terra," *J. Atmos. Ocean. Technol.*, vol. 25, no. 3, pp. 385–400, 2008.
[27] D. R. Doelling, V. Chakrapani, P. Minnis, and L. Nguyen, "The calibration of NOAA AVHRR visible radiances with VIRS," in *Proc. AMS 11th Conf. Satell. Meteorol. Oceanogr.*, Madison, WI, USA, Oct. 15–18, 2001, pp. 614–617.
[28] D. R. Doelling, L. Nguyen, and P. Minnis, "On the use of deep convective clouds to calibrate AVHRR data," in *Proc. SPIE*, 2004, vol. 5542, pp. 1–10.
[29] G. Thuillier *et al.*, "The visible solar spectral irradiance from 350 to 850 nm as measured by the SOLSPEC spectrometer during the ATLAS-1 mission," *Solar Phys.*, vol. 177, pp. 41–61, 1998.
[30] H. Neckel and D. Labs, "The solar radiation between 3300 and 12500 Å," *Solar Phys.*, vol. 90, no. 2, pp. 205–258, Feb. 1994.
[31] E. V. P. Smith and D. M. Gottlieb, "Solar flux and its variations," *Space Sci. Rev.*, vol. 16, no. 2, pp. 771–802, 1974.
[32] X. Xiong, "MODIS reflective solar calibration and uncertainty assessment," in *Proc. Joint Meet. GISCS Res. Data Work. Group*, Daejeon, Korea, Mar. 22–25, 2011, pp. 1–21.
[33] A. K. Heidinger, W. C. Straka, III, C. C. Molling, J. T. Sullivan, and X. Wu, "Deriving an inter-sensor consistent calibration for the AVHRR solar reflectance data record," *Int. J. Remote Sens.*, vol. 31, no. 24, pp. 6493–6517, Dec. 2010.
[34] R. Bhatt, D. R. Doelling, B. Scarino, A. Gopalan, and C. O. Haney, "An initial assessment of the VIIRS onboard calibration using DCC and desert referenced to the Aqua-MODIS calibration," in *Proc. SPIE Earth Observ. Syst. XVIII*, San Diego, CA, USA, 2013, vol. 8866, Art. ID. 88660K.
[35] D. R. Doelling, L. Nguyen, and P. Minnis, "Calibration comparisons between SEVIRI, MODIS, and GOES data," in *Proc. EUMETSAT Meteorol. Satell. Conf.*, Prague, Czech Republic, May 17–20, 2004, pp. 1–7.
[36] J. F. Meirink, R. A. Roebeling, and P. Stammes, "Inter-calibration of polar imager solar channels using SEVIRI," *Atmos. Meas. Technol.*, vol. 6, pp. 2495–2508, 2013.
[37] B. A. Wielicki *et al.*, "Clouds and the Earth's Radiant Energy System (CERES): An Earth observing system experiment," *Bull. Amer. Meteorol. Soc.*, vol. 77, no. 5, pp. 853–868, May 1996.
[38] D. R. Doelling *et al.*, "Geostationary enhanced temporal interpolation for CERES flux products," *J. Atmos. Ocean. Technol.*, vol. 30, no. 6, pp. 1072–1090, Jun. 2013.
[39] D. L. Morstad, D. R. Doelling, R. Bhatt, and B. Scarino, "The CERES calibration strategy of the geostationary visible channels for CERES cloud and flux products," in *Proc. SPIE, Earth Observ. Syst. XVI*, 2011, Art. ID. 815316.
[40] D. R. Doelling, R. Bhatt, D. Morstad, and B. Scarino, "Algorithm Theoretical Basis Document (ATBD) for ray-matching technique of calibrating GEO sensors with Aqua-MODIS for GSICS," https://gsics.nesdis.noaa.gov/pub/Development/AtbdCentral/GSICS_ATBD_RayMatch_NASA_2011_09.pdf
[41] D. R. Doelling, C. Lukashin, P. Minnis, B. Scarino, and D. Morstad, "Spectral reflectance corrections for satellite intercalibrations using SCIAMACHY data," *IEEE Geosci. Remote Sens. Lett.*, vol. 9, no. 1, pp. 119–123, Jan. 2012.
[42] B. Scarino *et al.*, "Using SCIAMACHY to improve corrections for spectral band differences when transferring calibration between visible sensors," in *Proc. SPIE*, 2012, vol. 8510, Art. ID. 85100Q.
[43] D. R. Doelling *et al.*, "The intercalibration of geostationary visible imagers using operational hyperspectral SCIAMACHY radiances," *IEEE Trans. Geosci. Remote Sens.*, vol. 51, no. 3, pp. 1245–1254, Mar. 2013.
[44] C. Cao, X. Xiong, and F. Weng, "Suomi NPP VIIRS SDR postlaunch calibration/validation: An overview of progress, challenges, and the way forward," in *Proc. SPIE*, 2012, vol. 8510, Art. ID. 851014.
[45] B. A. Wielicki *et al.*, "Achieving climate change absolute accuracy in orbit," *Bull. Amer. Meteorol. Soc.*, vol. 94, no. 10, pp. 1519–1539, Oct. 2013.

David R. Doelling received the B.S. degree in meteorology from The University of Utah, Salt Lake City, UT, USA, in 1985 and the M.S. degree in atmospheric science from the University of Washington, Seattle, WA, USA, in 1991.

He is currently a Senior Research Scientist with the NASA Langley Research Center, Hampton, VA, USA, where he is the Time Interpolation and Spatial Averaging Sublead for the Clouds and Earth's Radiant Energy System (CERES) Project and responsible for the diurnal averaging and spatial gridding of CERES footprint cloud and radiative flux parameters. He is also a member of the Geostationary Earth Radiation Budget Experiment and Megha-Tropique science teams, which are projects similar to CERES that measure broadband fluxes. He has studied the orbital sampling errors for proposed satellites as a member of the Climate Absolute Radiance and Refractivity Observatory Science Definition Team. He is the Global Space-based Inter-Calibration System NASA Representative and currently the Visible Calibration Lead. His research interests include geostationary imager calibration, diurnal averaging techniques of satellite observations, and satellite sampling studies.

Aisheng Wu received the B.S. degree in atmospheric science from the University of Science and Technology of China, Hefei, China, in 1983, the M.Sc. degree in atmospheric remote sensing from the Chinese Academy of Science, Lanzhou, China, in 1991, and the Ph.D. degree in biometeorology/soil physics from the University of British Columbia, Vancouver, BC, Canada, in 1999.

He is with both the MODIS and Visible/Infrared Imaging Radiometer Suite Characterization and Support Teams with the NASA Goddard Space Flight Center, Greenbelt, MD, USA, where he is currently the Technical Lead responsible for MODIS calibration algorithm development and validation.

Xiaoxiong (Jack) Xiong received the B.S. degree in optical engineering from the Beijing Institute of Technology, Beijing, China, and the Ph.D. degree in physics from the University of Maryland, College Park, MD, USA.

He is currently an Optical Physicist with the NASA Goddard Space Flight Center (NASA GSFC), Greenbelt, MD, currently serving as the MODIS Project Scientist and the Technical Lead for both the MODIS Characterization Support Team and the VIIRS Characterization Support Team. Before joining NASA GSFC, he had also worked in the fields of optical instrumentation, nonlinear optics, laser and atomic spectroscopy, and resonance ionization mass spectrometry at universities, industry, and the National Institute of Standards and Technology.

Benjamin R. Scarino received the B.S. and M.S. degrees in meteorology from the Pennsylvania State University, University Park, PA, USA, in 2008 and 2010, respectively. His graduate research was focused on the application of a Lagrangian objective analysis technique for obtaining 3-D thermodynamic output to a 2002 International H2O Project data set for the purpose of studying moisture and cloud variability in the boundary layer.

He is currently a Research Scientist with Science Systems and Applications, Inc., Hampton, VA, USA, where he supports work performed at the NASA Langley Research Center, specifically the development and improvement of the Clouds and the Earth's Radiant Energy System and Advanced Very High Resolution Radiometer global multispectral cloud property retrieval algorithms and geostationary/polar-orbiting satellite calibration and radiation property data set development projects. He is a specialist on intercalibration and trend analysis techniques for geostationary and polar-orbiting satellite instruments, whereby he develops signal-correction algorithms for inter-instrument spectral band differences using hyperspectral detectors and derives absolute calibrations for the satellite sensors.

Rajendra Bhatt received the B.S. degree in electronics engineering from Tribhuvan University, Kirtipur, Nepal, in 2002 and the M.S. degree in electrical engineering from South Dakota State University (SDSU), Brookings, SD, USA, in 2009. His graduate research at SDSU was focused on the consistent radiometric calibration of the Landsat 1 through 5 MSS sensors using pseudoinvariant Earth targets.

He is currently a Senior Researcher with Science Systems and Applications, Inc., Hampton, VA, USA, where he provides support to the NASA Langley Research Center with the Clouds and the Earth's Radiant Energy System Project by developing vicarious techniques of in-flight calibration of geostationary and low Earth orbiting satellite visible sensors to assess their performance on orbit and ensure the usability of climate data.

Conor O. Haney received the B.S. and M.S. degrees in atmospheric sciences from the University of Illinois at Urbana-Champaign, Champaign, IL, USA, in 2010 and 2013, respectively.

He is currently a Staff Research Scientist with Science Systems and Applications, Inc., Hampton, VA, USA, supporting NASA Langley Research Center contracts. He is primarily responsible for maintaining the real-time visible sensor calibration for geostationary satellites for the Clouds and the Earth's Radiant Energy System Project. He is currently developing and improving geostationary visible imager calibration techniques and monitoring their performance.

Daniel Morstad received the Bachelor's and Master's degrees in electrical engineering from South Dakota State University, Brookings, SD, USA, in 2007 and 2009, respectively. His graduate research focused on the development of a statistically based automation technique for selecting the most temporally invariant Earth targets based on the Landsat-5 Thematic Mapper data record.

During 2009 and 2012 he was with Science Systems and Applications, Inc. Hampton, VA, USA, in support of the Clouds and Earth's Radiant Energy System (CERES) project at NASA Langley Research Center, Hampton, VA, USA. He was primarily responsible for maintaining the real-time geostationary visible sensor calibration record and developing a deep convective cloud absolute calibration technique. Since 2013 he is a testing group engineer employed by Commonwealth Edison Company in Chicago, IL, USA.

Arun Gopalan received the B.S. degree in mechanical engineering from the University of Bombay, Mumbai, India, in 1991 and the M.S. degree in mechanical engineering from the State University of New York (SUNY), Stony Brook, NY, USA, in 1993. He has completed all Ph.D. requirements, excluding dissertation defense, as of 1997 at SUNY. His dissertation focused on the research and development of an optimal retrieval algorithm for simultaneous extraction of diurnal stratospheric nitrogen dioxide and aerosol extinction profiles using Earth limb infrared mission measurements from the NASA Upper Atmosphere Research Satellite CLAES instrument.

He is currently a Senior Research Scientist with Science Systems and Applications Inc., Hampton, VA, USA, in support of the NASA Langley Research Center's Clouds and the Earth's Radiant Energy System and Climate Absolute Radiance and Refractivity Observatory projects. He has worked in the area of satellite remote sensing for over 15 years with earth science research groups at the NASA Goddard Space Flight Center, Greenbelt, MD, USA, and National Center for Atmospheric Research, Boulder, CO, USA. He has coauthored a number of journal papers. His research interests include studies of postlaunch calibration techniques to understand satellite sensor performance, science retrieval algorithm development, remotely sensed data processing methods, aerosol–cloud–climate feedback mechanisms, and visualization of large-scale earth science data sets and data mining.